frontiers | Frontiers in Earth Science

TYPE Original Research
PUBLISHED 11 January 2023
DOI 10.3389/feart.2022.1018712

OPEN ACCESS

EDITED BY
Hao Zou,
Chengdu University of Technology, China

REVIEWED BY
Qingqiang Meng,
SINOPEC Petroleum Exploration and Production Research Institute, China
Bin Cheng,
China University of Petroleum, Qingdao, China
Hong Xiao,
China University of Petroleum, China

*CORRESPONDENCE
Zhijun Qin,
zhijunqin_karamay@126.com

SPECIALTY SECTION
This article was submitted to Economic Geology, a section of the journal Frontiers in Earth Science

RECEIVED 13 August 2022
ACCEPTED 30 September 2022
PUBLISHED 11 January 2023

CITATION
Qin Z, Qi H, Liang Z, Ma W, Wang R and Wu W (2023), Geochemical classification and secondary alteration of crude oil in the southern thrust belt of Junggar Basin.
Front. Earth Sci. 10:1018712.
doi: 10.3389/feart.2022.1018712

Geochemical classification and secondary alteration of crude oil in the southern thrust belt of Junggar Basin

Zhijun Qin[1]*, Hongyan Qi[1], Zeliang Liang[1], Wanyun Ma[2], Ruiju Wang[3] and Wei'an Wu[3]

[1]Research Institute of Petroleum Exploration and Development, Xinjiang Oil Company, PetroChina, Karamay, China, [2]Research Institute of Experiment and Testing, Xinjiang Oil Company, PetroChina, Karamay, China, [3]Research Institute of Petroleum Exploration and Development, PetroChina, Beijing, China

This study analyzed, 18 oil samples from four representative oil-bearing secondary tectonic units in the southern thrust belt of the Junggar Basin. The genetic types and the secondary alteration of oil were discussed based on the characteristics of light hydrocarbon compounds, adamantanes, sterane/terpene biomarkers, and stable carbon isotopic composition of the bulk oil. . The results show that the oil in the study area can be divided into five categories. Type I oil is characterized by ^{13}C-depleted carbon isotopes, a low pristane to phytane ratio, and high gammacerane and low diasterane content, whereas Type II oil exhibits the opposite characteristics. Type III is very similar to Type II oil but has a higher ^{13}C-depleted bulk carbon isotopic composition and a wider carbon number of tricyclic terpenes. Type IV and V oils are similar to Type I oils, except for relatively lower gammacerane content. Further, Type IV oils also have high ααα 20R regular sterane content, ^{13}C-enriched bulk oil carbon isotopes, and a higher pristane to phytane ratio than Type I oil. In contrast, the relative content of C_{27} regular steranes of Type V oils is considerably lower than that of Type I oils. The oil in the study area has not suffered from biodegradation. Maturity information indicated by regular biomarkers (i.e., steroid, terpene, and phenanthrene) and adamantane differs significantly, with the latter exhibiting a strong cracking characteristic. This reflects the charging and mixing of oils formed at different evolution stages. The other types of oils are in the normal oil-generating window and do not suffer from intense cracking. The oil in the study area is generally subjected to evaporative fractionation, but there are obvious differences in the degree of alteration between different oil-bearing structures and different reservoirs with the same structure. This study is of great significance for understanding the origin and accumulation process of oil and gas in a complex structural zone.

KEYWORDS

biomarker, carbon isotope, origin and genetic type, secondary alteration, southern thrust belt, Junggar Basin

1 Introduction

The southern thrust belt (STB) in the Junggar Basin is rich in oil and gas resources, and many oil and gas fields have been discovered since the discovery of the Dushanzi oilfield. In recent years, the successful breakthroughs of Wells Gaotan 1, Huotan 1, and Tianwan 1 have revealed broad oil and gas prospects in the STB (Du et al., 2019; He et al., 2019; Wang et al., 2021). Complex types of oil and gas have been found in the STB, including heavy oil, normal oil, light oil, condensates, and natural gas. The oil-producing strata are vertically distributed from Triassic to Neogene. Several sets of potential source rocks in this area overlap each other in the plane. Their maturity and hydrocarbon generation and expulsion history are significantly different. The geochemical characteristics of oil from different tectonic units or oil fields in the same tectonic unit are complex with several different origins (Guo et al., 2005; Chen et al., 2016a,b). Despite extensive research on the geochemical characteristics of source rocks, the geochemical characteristics and classification of oil, and the sources of oil and gas in the STB, there remains a lack of consensus (Zhang et al., 2003; Li et al., 2004; Guo et al., 2005; Wei D. et al., 2007; Cao et al., 2010; Chen et al., 2015a; Chen et al., 2016a). In addition, little attention has been paid to the secondary alteration of oil in this area and its implications for the petroleum accumulation process (Lu et al., 2019). Therefore, this study conducted a detailed geochemical anatomy of 18 oil samples collected from key oil-bearing structural units of the STB. Based on the characteristics of light hydrocarbons, adamantanes, biomarkers, and stable carbon isotopic composition of the bulk oil ($\delta^{13}C_{bulk}$), the geochemical classification and potential secondary alterations such as biodegradation, thermal cracking, and evaporative fractionation were discussed to better understand the genesis and accumulation process of multiple types of oil in this area.

2 Geological background

The STB spreads in an east-west direction and contains six second-order structural units from west to east, including the Sikeshu sag, Gaoquan tectonic belt, Aika anticline belt, Huomatu arc anticline belt, Qigu bruchfalten, and Fukang bruchfalten (Figure 1). The formation and evolution of the STB are closely related to the North Tianshan Orogenic Belt. The STB has experienced three tectonic evolution stages: the Permian foreland basin, the Triassic-Paleogene intracontinental depression, and the Neogene-Quaternary proterozoic continental basin (Gong et al., 2018; 2019). Many large anticlinal structures have been developed, and overlapping composite petroleum systems have been formed (He et al., 2019). The thrust nappe deformation is the main structural deformation mode in the thrust belt, and three rows of structural belts are formed from the piedmont basin of the orogenic belt in a nearly east-west direction, showing the typical characteristics of "north-south" zoning and "east-west" segmentation (Xiao et al., 2012; He et al., 2019). The strata of the STB have been continuously deposited since the Permian period, including Permian, Triassic, Jurassic, Cretaceous, Paleogene, and Quaternary, with a total thickness of 10–15 km (Chen et al., 2015a; Gong et al., 2018). Several sets of potential source rocks, such as Paleogene, Cretaceous, Jurassic, Triassic, and Permian, were developed with a considerable thickness (Figure 2). The lithology of the source rock is mainly dark mudstone, and the Jurassic and Triassic source rocks also developed carbonaceous mudstone and coal (Li et al., 2003; Chen et al., 2015a) (Figure 2). Exploration practice confirmed that the upper, middle, and lower reservoir and cap assemblages developed in the STB (Figure 2). The upper assemblage is composed of reservoirs in the Neogene

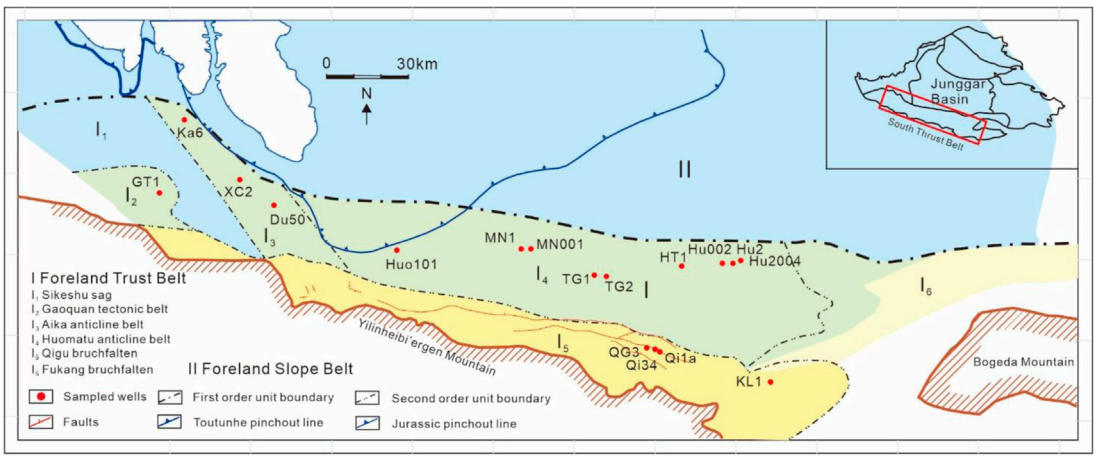

FIGURE 1
Map showing the structural units of STB and the location of sampled wells.

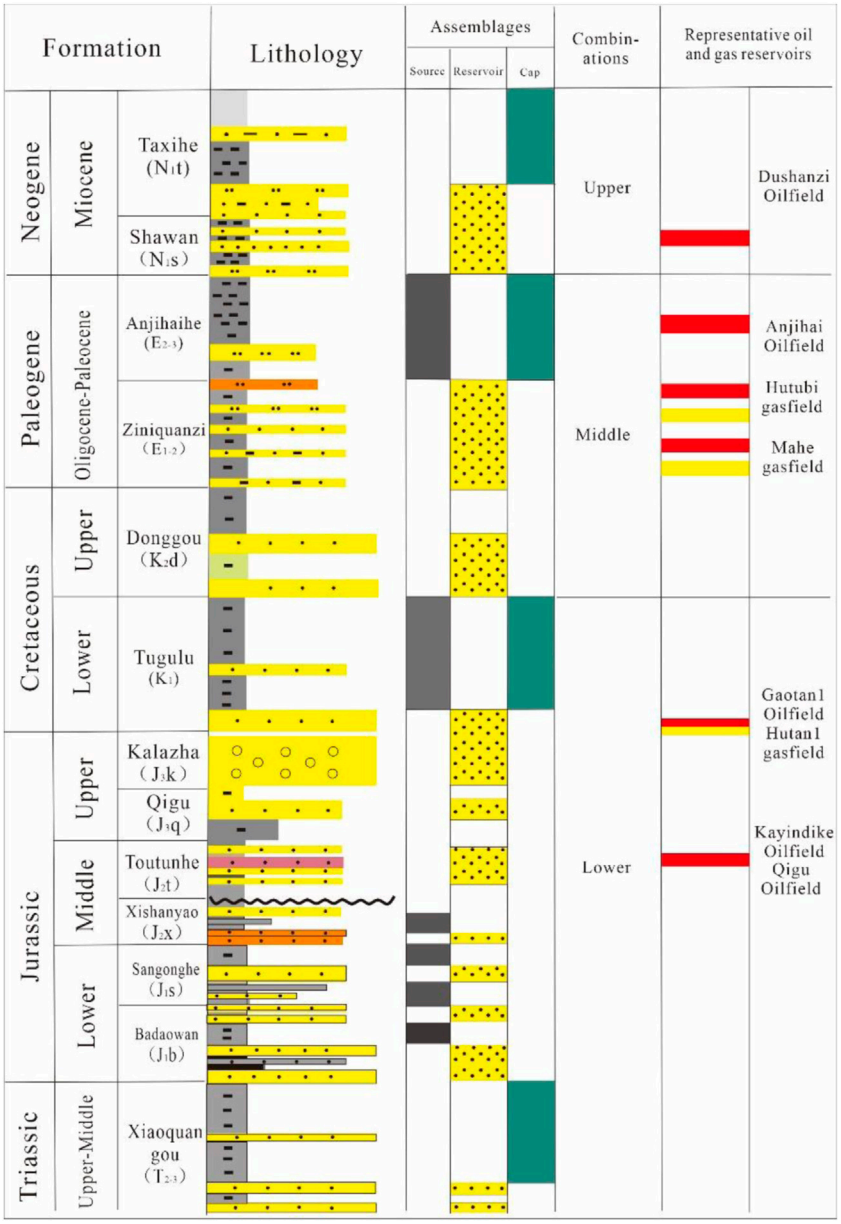

FIGURE 2
Stratigraphic chart and source-reservoir-cap assemblages in the STB of the Junggar Basin.

Dushanzi and Taxihe Formations and mudstone cap rocks of the Taxihe Formation; the middle assemblage is composed of reservoirs in the Anjihaihe and Ziniquanzi Formations and cap rocks in the Anjihaihe Formation; the lower assemblage consists of reservoirs in the Jurassic Badaowan, Sangonghe, Xishanyao, and Toutunhe Formations, Cretaceous Qingshuihe Formation, and mudstone caprocks in the Cretaceous Tugulu Group (Li et al., 2003; Du et al., 2019) (Figure 2). Several oil and gas resources have been found in different reservoir–cap assemblages (Gong et al., 2019).

3 Samples and methods

A total of 18 oil samples were collected from the Gaoquan tectonic belt, Aika anticline belt, Huomatu anticline belt, and Qigu bruchfalten in the STB. The oil-producing horizons include Triassic, Jurassic, Cretaceous, Paleogene, and Neogene. The well location is depicted in Figure 1.

After adding petroleum ether into a 50-mg oil sample to precipitate asphaltene, the sample was separated into saturated hydrocarbon, aromatic hydrocarbon, and non-

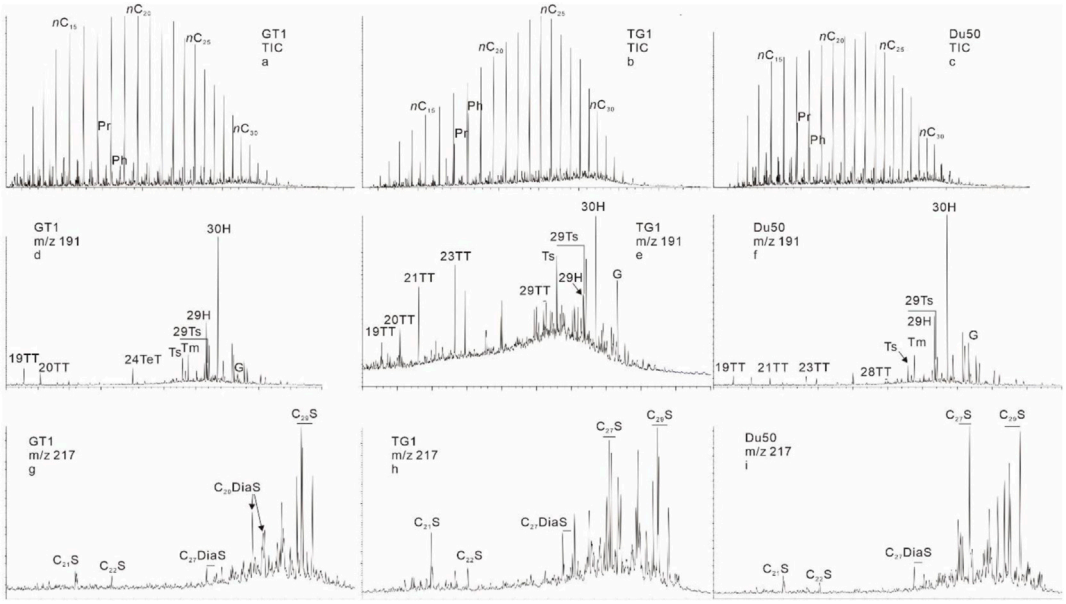

FIGURE 3
(A–C) TIC of saturated hydrocarbons showing distributions of *n*-alkanes and acyclic isoprenoids; **(D–F)** M/z 191 mass chromatograms showing distributions of terpanes; **(G–I)** M/z 217 mass chromatograms showing distributions of steranes. Pr: pristane; Ph: phytane; TT: tricyclic terpane, TeT: tetracyclic terpane, Ts: 18α (H)-trinorhopane; Tm: 17α (H)-trinorhopane; H: hopane, G: gammacerane; S: regular sterane; DiaS: diasterane.

hydrocarbon fractions by column chromatography filled with alumina and silica gel. The corresponding fractions were eluted by petroleum ether, a dichloromethane/petroleum ether mixture (2:1, V/V), and ethanol, respectively. The saturated and aromatic hydrocarbon fractions were analyzed by gas chromatography–mass spectrometry (GC–MS) using Agilent Intuvo 9000 GC and 5977BMS. Chromatography was performed on an HP–5MS capillary column (60 m × 0.25 mm × 0.25 μm) with helium as the carrier gas. The ion source of MS was electron bombardment (EI) with an ionization voltage of 70 eV, using two modes: full scan and selective ion scan. For the saturated hydrocarbon fraction, quantitative d_4-αααC_{29}20R sterane as an internal standard was added. The chromatograph furnace temperature was initially set at 50°C, 1 min after 20°C/min heating to 120°C, then 3°C/min heating to 310°C and constant temperature for 25 min. The d_8-dibenzothiophene was added to the aromatic hydrocarbon fraction as an internal standard. The furnace temperature was initially set at 80°C, a constant temperature for 1 min; then, the temperature was increased to 310°C at 3°C/min for 16 min. The saturated hydrocarbon fractions of representative samples were analyzed by metastable ion-monitoring GC–MS using Agilent 6890 GC, along with Quatro II MS. Chromatography was performed on a DB–5 capillary column (60 m × 0.25 mm × 0.25 μm) with helium as the carrier gas. The temperature of the chromatographic furnace was initially set at 100°C, then it was heated to 320°C at 4°C/min for 1 min, and the temperature remained constant for 20 min. EI was used as the ion source of MS, the ionization voltage was 70 eV, and the metastable reaction monitoring mode was employed.

In addition, an overall chromatographic analysis was performed on the oil samples using an Agilent 8,890 gas chromatograph, equipped with an HP–PONA capillary column (50 m × 0.2 mm × 0.5 μm), at an initial furnace temperature of 35°C, the constant temperature after 5 min at 3°C/min was increased to 70°C, and then the temperature was increased to 300°C at 4.5°C/min for 35 min. An Agilent Intuvo 9,000 gas chromatograph and a 5977B mass spectrometer were used to analyze the diamondoid series. The chromatogram was configured with HP–5MS capillary column (60 m × 0.25 mm × 0.25 μm), and the mass spectrum was selected through the ion scanning mode. The initial temperature of the chromatographic furnace was 50°C. After 1 min, the temperature was increased to 250°C at 3°C/min and then to 310°C at 20°C/min for 10 min d_{16}-adamantane was added to the oil sample as an internal standard to calculate the absolute content of the compound. Following PDB standards, the $\delta^{13}C_{bulk}$ ratios were determined using a FLASH 2000 EA–MAT 253 IRMS stable carbon isotope ratio mass spectrometer.

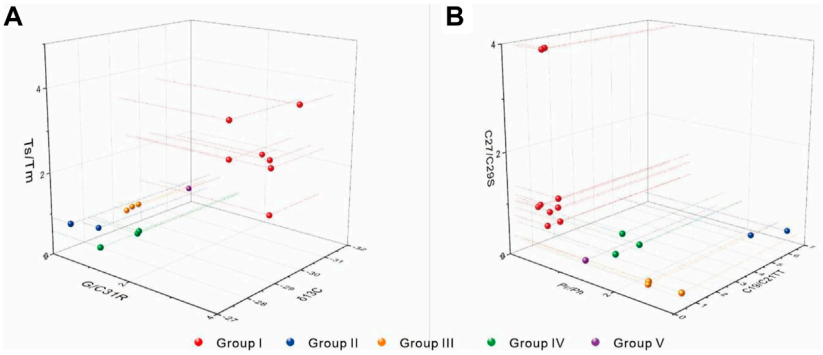

FIGURE 4
3-D scatter plots of **(A)** (x) $\delta^{13}C$, (y) Ts/Tm, and (z) $G/C_{31}R$ and **(B)** (x) C_{19}/C_{21} tricyclic terpane, (y) C_{27}/C_{29} steranes, and (z) pristane/phytane showing classification of genetic groups for studied oil samples.

4 Results

4.1 Group composition and stable carbon isotopes of bulk oil

The density of oil in the STB varies significantly from 0.76 to 0.90 g/cm^3. The composition of most oil groups is dominated by saturated hydrocarbons, and the content of non-hydrocarbon and asphaltene is low. Some oils do not contain asphaltene components. The percentages of saturated hydrocarbons, aromatic hydrocarbons, and non-hydrocarbon + asphaltene are 47.3%–88.7%, 2.81%–15.9%, and 4.94%–44.5%, respectively. There was a good negative correlation between the content of saturated hydrocarbons and non-hydrocarbon + asphaltene. The oil from Wells KL1 and Huo101 had the highest oil density, the lowest saturated hydrocarbon content, and the highest non-hydrocarbon + asphaltene content. The sample density correlated well with the chemical composition.

The $\delta^{13}C_{bulk}$ ratios also varied greatly, ranging from −31.4‰− to −27.0‰, reflecting the diversity of oil properties and the complex sources of the oil. Further, the $\delta^{13}C_{bulk}$ ratios from different tectonic units as well as the $\delta^{13}C_{bulk}$ ratios from different production layers of the same tectonic unit exhibit significant differences. On the other hand, oils from adjacent tectonic units have very similar $\delta^{13}C_{bulk}$ ratios. Based on the oil samples analyzed in this study, there are obvious differences in $\delta^{13}C_{bulk}$ ratios among the oils from different structural belts. The oil in the Aika anticline belt and its western tectonic units is more enriched in ^{13}C than in the eastern Huomatu anticline belt and Qigu bruchfalten.

4.2 C_5–C_7 light hydrocarbon compounds

Light hydrocarbons are important components of oil, especially for light oil and condensate, where light hydrocarbon compounds can account for up to 90% of the total oil mass (Wang, 2011). The relative light hydrocarbon content in oils in the STB varies greatly, ranging from 0% to 73.7%. Oil from Well HT1 exhibited the highest light hydrocarbon content, accounting for 73.7% of the total oil mass, whereas oil from Well KL1 exhibited the lowest light hydrocarbon content, almost losing all of them. In addition, the distribution of light hydrocarbon compounds varied significantly among samples, especially the relative abundance of toluene. For example, oil from Well Hu2004 exhibited very high toluene content, whereas that from Well GT1 exhibited relatively low abundance, with the Tol/nC_7 ratio ranging from 0.64 to 5.32.

4.3 Adamantanes

The oil samples contained varying amounts of adamantane series compounds, primarily monoadamantane, diamantine, and their alkyl-substituted isomers. Monoadamantane was the most abundant, and methyl adamantane was the absolute dominant compound. The total content of adamantanes varied significantly among the samples, ranging from 134.9 to 3,174.8 ppm (μg/g of total oil). The total content of monadamantanes and diamantanes was 88.4–2,779.8 ppm and 14.3–395.0 ppm, respectively. Both 3- and 4-methyldiamondotane were detected in the samples, but their abundance differs significantly, with their total content being 5.75–174.5 ppm.

TABLE 1 Summarized ranges and averages of biomarker parameters and whole oil/extracts carbon isotopes for sample groups.

Groups	$\delta^{13}C$/‰	Pr/Ph	C_{19}/C_{21} TT	$C_{24}TeT/C_{26}TT$	Ts/Tm	$C_{29}Ts/C_{29}H$	$C_{30}DiaH/C_{30}H$	G/$C_{31}R$	C_{27}/C_{29} S	C_{27}/C_{29} DiaS
I	−31.4 – −29.3 −30.1	0.45 – 0.90 0.67	0.24 – 0.65 0.38	0.18 – 0.52 0.30	1.11 – 3.66 2.45	0.55 – 1.39 0.82	0.17 – 0.92 0.49	2.26 – 4.81 3.21	0.74 – 3.96 1.67	0.78 – 3.70 1.87
II	−27.9 – −27 −27.5	2.55 – 2.74 2.65	5.29 – 6.83 6.06	8.95 – 12.1 10.5	0.52 – 0.91 0.72	0.19 – 0.29 0.24	0.16 – 0.25 0.20	0.46 – 0.52 0.49	0.24 – 0.34 0.29	0.18 – 0.20 0.19
III	−29.4 – −29 −29.2	2.40 – 2.91 2.58	0.42 – 0.62 0.52	1.61 – 2.24 1.9	0.65 – 0.72 0.69	0.24 – 0.27 0.26	0.13 – 0.15 0.14	0.37 – 0.40 0.39	0.21 – 0.25 0.23	0.28 – 0.31 0.30
IV	−28.2 – −27 −27.8	1.61 – 1.89 1.79	0.36 – 1.52 1.10	0.89 – 1.82 1.50	0.57 – 0.65 0.60	0.23 – 0.27 0.25	0.11 – 0.15 0.13	1.28 – 1.36 1.32	0.56 – 0.70 0.62	0.48 – 0.69 0.62
V	-30.7	1.42	0.18	0.58	0.91	0.24	0.11	0.81	0.34	0.47

Pr/Ph: pristane/phytane; TT: tricyclic terpane; TeT: tetracyclic terpane; Ts: 18α (H)-trinorneohopane; Tm: 17α (H)-trinorhopane; $C_{29}Ts/C_{29}H$: C_{29} norneohopane/C_{29} hopane; $C_{30}DiaH/C_{30}$ H: C_{30} diahopane/C_{30} hopane; G/$C_{31}R$: gammacerane/C_{31} hopanes 22R; S: regular sterane; DiaS: diasterane; Numerator: parameter range of minimum to maximum value, Denominator: average value.

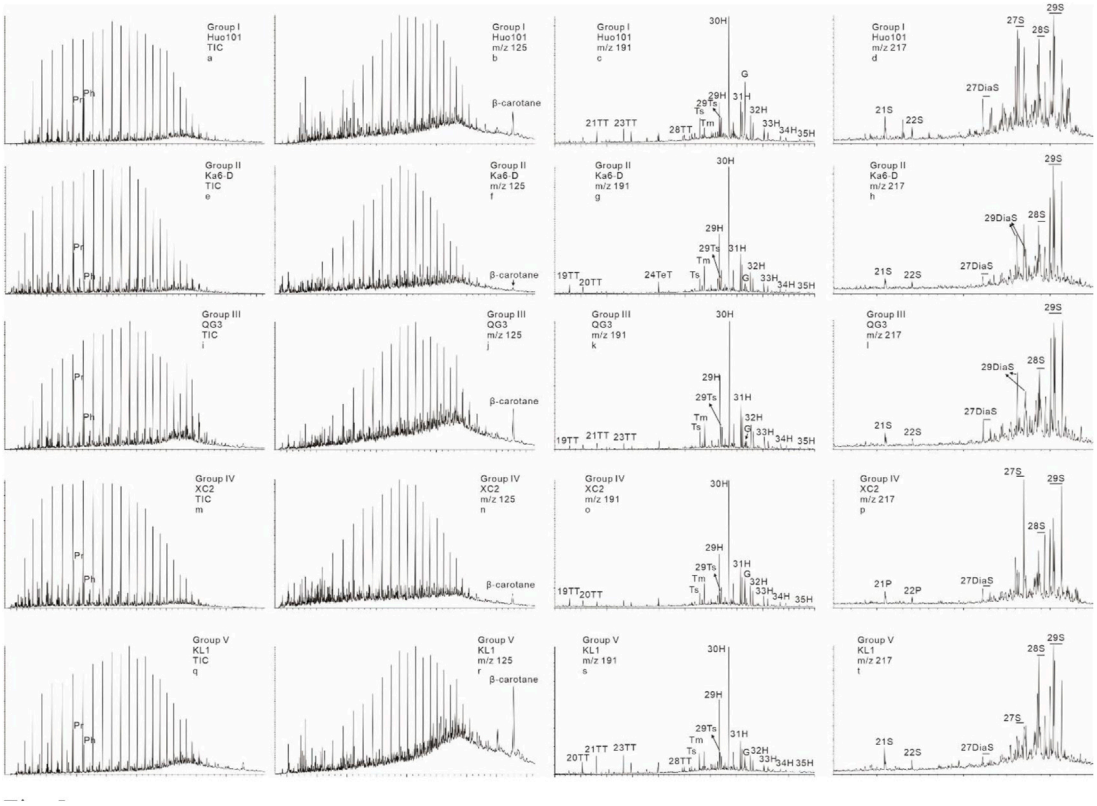

FIGURE 5
Summarized TIC, m/z 125, m/z 191, and m/z 217 mass chromatograms of saturated hydrocarbons showing distributions of *n*-alkanes and acyclic isoprenoids, β-carotane, terpanes, and steranes for **(A–D)** Group I oil; **(E–H)** Group II oil; **(I–L)** Group III oil; **(M–P)** Group IV oil; **(Q–T)** Group V oil. The abbreviations of compound names see Figure 3.

4.4 Biomarkers

4.4.1 n-alkanes and isoprenoids

The analyzed samples contain abundant *n*-alkanes, and the carbon number ranges from C_{11} to C_{36} (Figures 3A–C). The normal alkane series exhibits a unimodal distribution, with the main-peak-carbon number ranging from C_{17} to C_{25}, and the ratio of C_{21-}/C_{22+} varies significantly, ranging from 0.52 to 3.47. There is no odd and even carbon number advantage, and the OEP is close to 1. Pristane (Pr) and phytane (Ph) were the dominant

isoprenoids, and their relative abundance varied significantly among the samples, with Pr/Ph ratios ranging from 0.45 to 2.91. Some oils (e.g., oil from Well GT1) had high Pr/Ph ratios, typically greater than 2; some oils (e.g., oil from Well TG1) had low Pr/Ph ratios, mostly less than 1. Other oils have Pr/Ph ratios between the two groups s (e.g., oil from Well Du50). In addition, β-carotene was also detected in the oils with different abundances.

4.4.2 Terpene

The terpenes of the oil in the STB are primarily dicyclic sesquiterpenes, tricyclic terpenes, C_{24} tetracyclic terpenes, and pentacyclic triterpenes. 13β (H),14α (H)-tricyclic terpenes were detected in all samples, but the relative abundance and carbon number distribution range of tricyclic terpenes differed significantly among the samples. The relative content of tricyclic terpenes in some oil samples such as Well GT1 is significantly lower than that of hopanes. Among the tricyclic terpenes, C_{19} and C_{20} tricyclic terpenes dominate, and the content of high-carbon-number isomers is very low or even difficult to detect, whereas the relative content of C_{24} tetracyclic terpenes is very high. In contrast, in some oil samples such as Well TG1, the relative content of tricyclic terpenes is very high, consistent with hopanes. The carbon number of tricyclic terpenes is widely distributed, C_{19}–C_{29} tricyclic terpenes are detected, and C_{23} tricyclic terpenes are mostly the main peak. The relative content of C_{19}, C_{20}, and C_{24} tricyclic terpenes is very low. Some oil samples, such as oil from Well Du50, exhibit a relatively low content of tricyclic terpenes, but the carbon number distribution is wide. In these oils, C_{19}–C_{29} tricyclic terpenes are detected, and the relative content of C_{19}–C_{23} tricyclic terpenes does not differ, whereas the relative content of C_{24} tetracyclic terpenes is high (Figures 3D–F). Pentacyclic triterpenes such as C_{27} neohopanes (Tm), C_{27}-rearranged neohopanes (Ts), C_{29}–C_{35} hopanes, C_{30}-rearranged hopanes, and gammacerane were detected in the oil samples. The distribution characteristics of pentacyclic triterpenes significantly differed among the samples, primarily in the relative abundance of Ts, C_{29}-rearranged neohopane (C_{29}Ts), C_{30}-rearranged hopane, and gammacerane (Figures 3D–F), which can be used as powerful indicators to distinguish the oil samples.

4.4.3 Sterane

The steranes detected in oils in the STB included progesteranes, homoprogesteranes, C_{27}–C_{29} diasteranes, and regular steranes (Figures 3G–I). The distribution characteristics of steranes also differ significantly among the oils, primarily reflected in the relative content of C_{27} and C_{29} steranes (both rearranged and regular steranes). Some oil such as oil from Well GT1 exhibit low C_{27} regular sterane content but very high C_{29} diasterane content. On the contrary, oil such as that from Well TG1 has a very high content of C_{27} regular steranes but low content of C_{29} diasteranes. The difference between the two can be used as a typical index to distinguish the oil samples. In addition, the relative abundances of different configuration compounds of regular steranes also vary significantly. For example, oil from Well XC2 exhibits an extremely high ααα20R configuration of regular steranes.

5 Discussion

5.1 Geochemical classification of oil

Combining the biomarker fingerprints and the $\delta^{13}C_{bulk}$ ratios, the oil in the STB can be divided into five types (Figure 4).

5.1.1 Type I oil

Type I oil has the lightest stable carbon isotopic composition, with $\delta^{13}C_{bulk}$ values ranging from −31.4 to −29.3‰ (Table 1). Ph was dominant in isoprenoids, and the Pr/Ph ratio was low, indicating that the lacustrine algae organic matter or the oil-prone parent material was deposited in a reductive environment. β-carotene was found in high abundance in most Type oils (Figures 5A,B). Tricyclic terpenes tend to be relatively high in abundance and have a wide distribution of carbon numbers. C_{28}, C_{29}, and C_{29+} tricyclic terpenes are commonly found in Type I oil. C_{23} tricyclic terpenes typically dominated the distribution of tricyclic terpenes, C_{21} tricyclic terpenes were also high, and C_{19} and C_{20} tricyclic terpenes were very low (Figure 5C). Besides, the abundance of C_{24} tetracyclic terpenes was relatively low, with a C_{24} tetracyclic terpene/C_{26} tricyclic terpene ratio ranging from 0.18 to 0.52 (Table 1). Among the distribution of pentacyclic triterpenes, C_{30} hopane is the primary peak, whereas the abundance of the other hopanes is relatively low. The relative content of Ts is higher than that of Tm, and the relative content of gammacerane is very high, typically higher than that of C_{31} hopane. The gammacerane/C_{31}hopane22R ratio is between 2.19 and 3.55 (Table 1), which is significantly higher than that of the other types of oil. Gammacerane is a landmark biomarker in saline lakes or stratified water with high salinity. Along with its high carotenane abundance and low Pr/Ph ratio, Type I oil reflects the organic matter deposited in a brackish and reducing environment (Brassel et al., 1985; Moldowan et al., 1985; Grice et al., 1998). In the distribution of steranes, the relative content of progesteranes and homoprogesteranes was low, and regular steranes were dominated by C_{27} and C_{29} steranes, with low C_{28} sterane content. The configuration of ααα C_{27}–C_{29}20R regular steranes exhibited a "V"-shaped distribution (Figure 5D), and the relative diasterane content was significantly lower than that of regular steranes. Type I oil includes oils from Wells Huo101, MN1, Hu 2004, and TG1, primarily distributed in the Huomatu anticline belt.

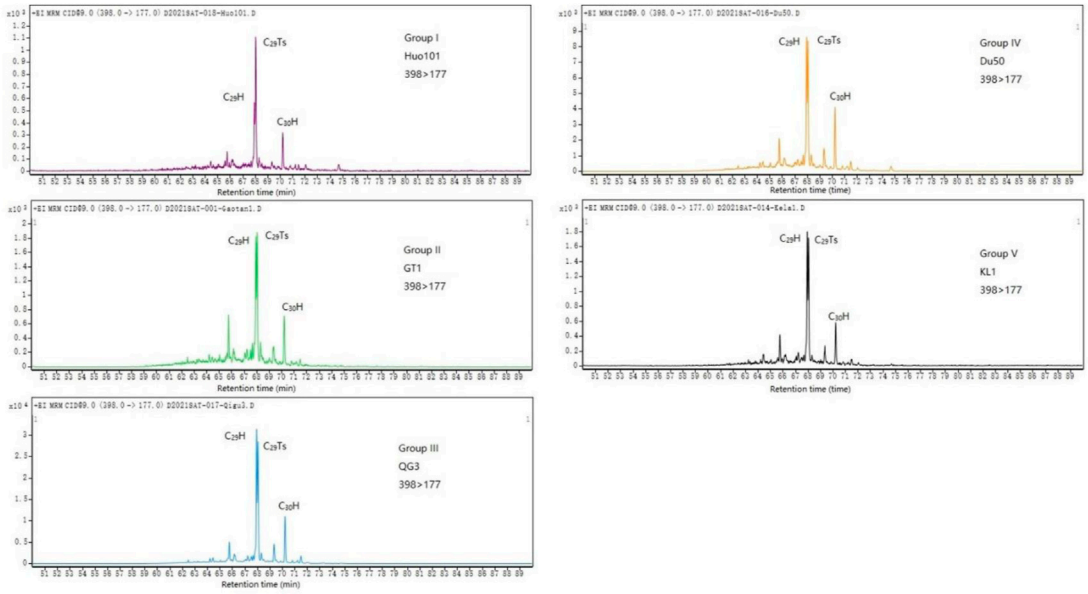

FIGURE 6
MRM chromatograms showing absence of 25-norhopanes in representative Group I–V oils. The abbreviations of compound names see Figure 3.

5.1.2 Type II oil

Type II oil has a more ^{13}C-enriched $\delta^{13}C_{bulk}$ ratio varying from −28.2 to −27.0‰ (Table 1) than Type I oil. The isoprenoid is dominated by Pr, and the Pr/Ph ratio is high, reflecting that their parent organic matter is dominated by terrigenous higher plants and deposited in an oxidation environment. It seldom contains β-carotene (Figures 5E,F). Generally, Type II oil exhibits relatively low tricyclic terpene content, whose distribution patterns are dominated by C_{19} and C_{20} tricyclic terpenes, with very low content of the other higher-carbon-number tricyclic terpenes (Figure 5G). This oil type has a high C_{19}/C_{21} tricyclic terpene ratio, ranging from 4.92 to 7.41 (Table 1). Owing to the low (or even undetected) C_{26} tricyclic terpene content, this oil type has a high C_{24}tetracyclic terpene/C_{26}tricyclic terpene ratio, ranging from 8.98 to 16.66 (Table 1). In pentacyclic triterpenes, the relative abundance of Ts was lower than that of Tm, and the Ts/Tm ratios were all less than 1; the primary peak of C_{30} hopanes is obvious, and the abundance of C_{29} and C_{31} hopanes was higher than that of C_{30} hopanes. In addition, the relative gammacerane content of Type II oil is generally low, with the gammacerane/C_{31}22Rhopane ratios mostly below 0.5 (Table 1). In the distribution of steranes, the content of C_{27} and C_{28} steranes was lower than that of C_{29}, dominating the distribution of steranes. Diasteranes were relatively abundant, with a high abundance in C_{29} diasteranes and low abundance in C_{27} diasteranes (Figure 5H). Type II oil includes Jurassic reservoir oil from Wells GT1 and Ka6, which is distributed in the western section of the study area.

5.1.3 Type III oil

Types III and II oils exhibited very similar distribution characteristics of isoprenoids, tetracyclic terpenes, gammacerane, and steranes but exhibited different $\delta^{13}C_{bulk}$ ratios, tricyclic terpenes distribution patterns, and β-cartane abundance (Figure 5I–L). Types III oil has relatively ^{13}C-depleted $\delta^{13}C_{bulk}$ ratios varying from −29.4 to −29.0‰ (Table 1). The relative content of tricyclic terpenes is very low, but the carbon number distribution is broad, from C_{19} to C_{26}. Extremely low content of C_{28} and C_{29} tricyclic terpenes may also exist. Among the C_{19}–C_{26} tricyclic terpenes, C_{21} and C_{23} tricyclic terpenes were dominant, whereas the abundance of the other tricyclic terpenes was slightly low (Figure 5K). The C_{19}/C_{21}tricyclic terpene ratios were 0.42–0.62 (Table 1). Type III oil includes Jurassic reservoir oil from Wells QG3, Qi34, and Qi1 in the Qigu bruchfalten.

5.1.4 Type IV oil

The distribution characteristics of hopanes and steranes in Type IV oil are generally similar to those of Type I oil. However, Type IV oil has relatively low gammacerane/C_{31}hopane22R ratios and high ααα20Rsteranes abundance in C_{27}–C_{29} regular steranes (Figures 5O and P). In addition, Type IV oil has relatively ^{13}C-enriched $\delta^{13}C_{bulk}$ ratios and a higher Pr/Ph ratio (Table 1) than Type I oil. Although the content of tricyclic terpenes is generally low, the carbon number distribution is wide, ranging from C_{19} to C_{29}. The abundance of C_{28} and C_{29} tricyclic terpenes is low, and the ratio of C_{19}/C_{21} tricyclic terpenes

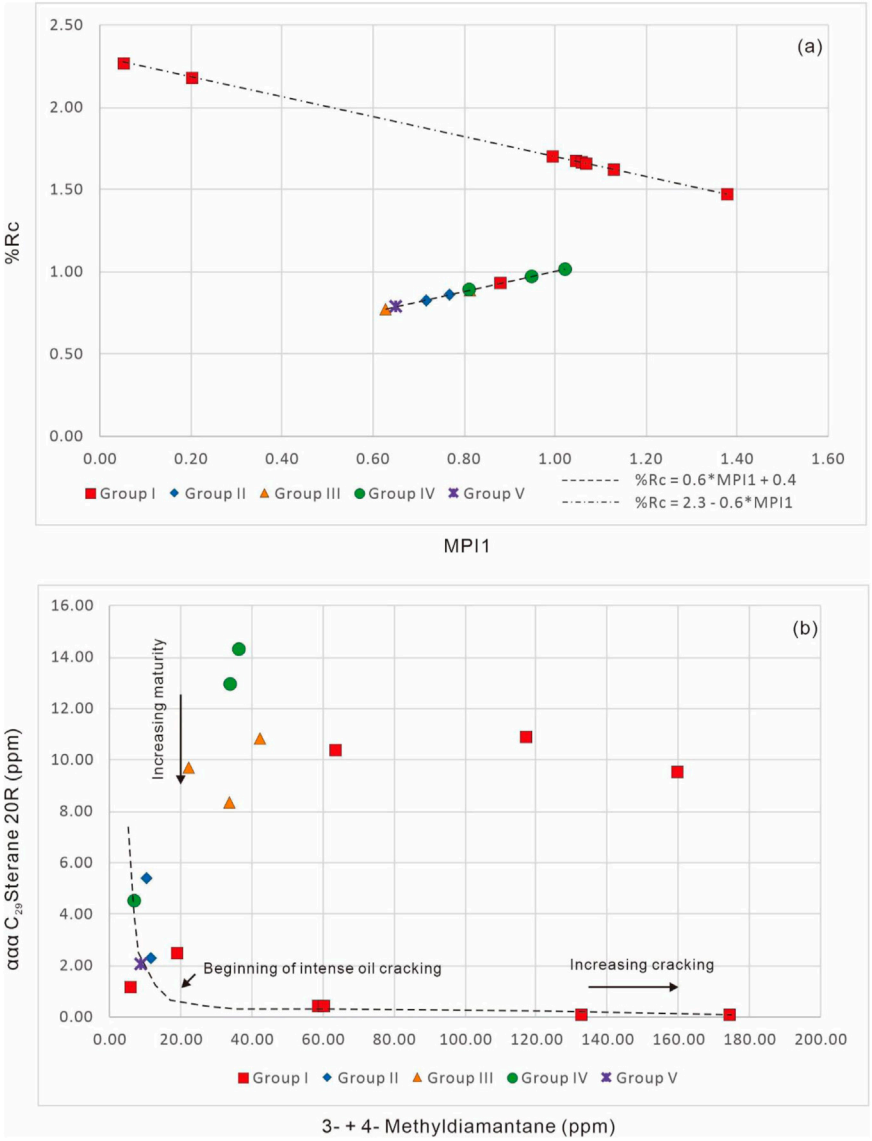

FIGURE 7
Crossplot of **(A)** MPI1 *versus* %Rc; **(B)** concentrations of 3- + 4-methyldiamantane *versus* those of ααα C_{29} sterane 20R.

varies greatly, ranging from 0.36 to 1.52 (Table 1). The content of C_{24} tetracyclic terpenes in Type IV oil was high, with the C_{24} tetracyclic terpene/C_{26} tricyclic terpene ratios ranging from 0.89 to 1.82 (Table 1). Type IV oil includes Neogene reservoir oil from Wells XC2, Du50, and Ka6, collected from the shallow strata of the Aika anticline belt.

5.1.5 Type V oil

Type V oil is collected from Well KL1, exhibiting Pr dominance with relatively high β-carotene content (Figures 5Q,R). The tricyclic terpenes, C_{24} tetracyclic terpenes, hopanes, and gammacerane of this oil sample are similar to those of Type I oil (Figure 5S). The relative gammacerane content of the KL1 oil was slightly lower than that of Type I oil (Table 1). In addition, the relative content of C_{27} regular steranes in C_{27}–C_{29} regular steranes is much lower than that of Type I oil, and the configuration of C_{27}–C_{29} ααα20R regular steranes in Type V oil show an inverse "L" shape distribution (Figure 5T).

5.2 Maturity and cracking of oil

With the increase in the burial depth, the increase in reservoir temperature will lead to the cracking of compounds in oil. Oil

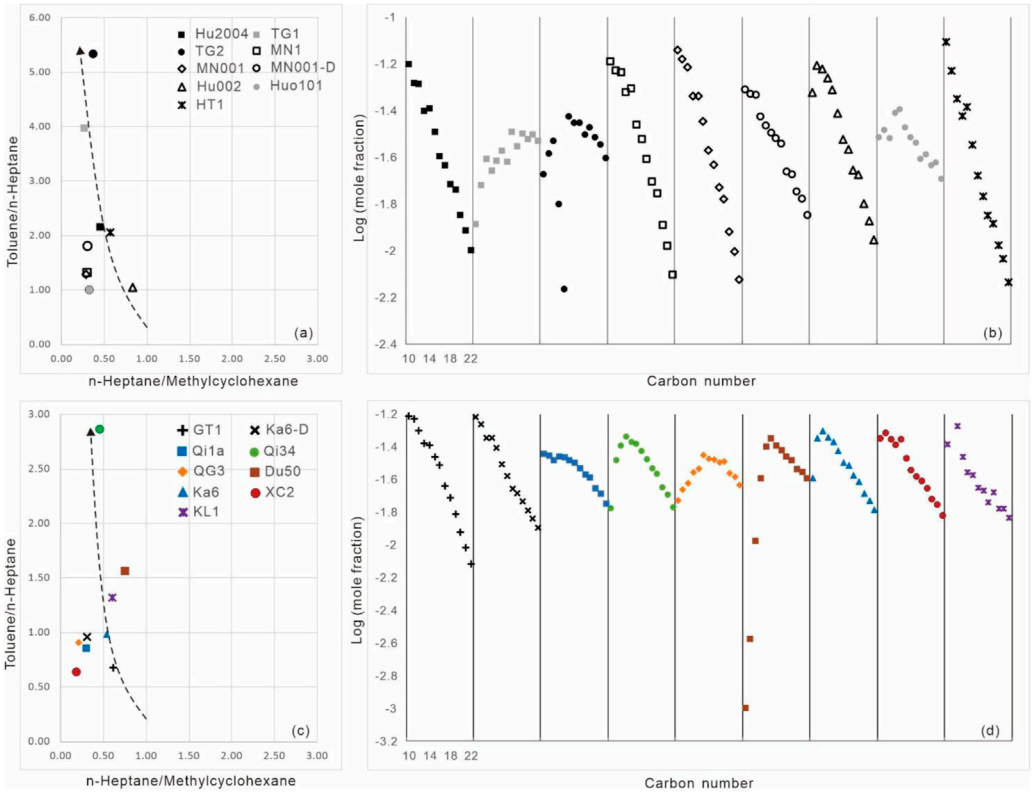

FIGURE 8
Crossplots of **(A)** the toluene/*n*-heptane *versus* *n*-heptane/methylcyclohexane and **(B)** carbon number *versus* the log of mole fraction for the C_{10}–C_{22} *n*-alkanes for Group I oils; **(C)** the toluene/*n*-heptane *versus* *n*-heptane/methylcyclohexane and **(D)** carbon number *versus* the log of mole fraction for the C_{10}–C_{22} *n*-alkanes for Group II–V oils.

maturity is an important index to judge whether it has reached the cracking stage. In this study, the isomerization maturity parameters 22S/(22S + 22R) of C_{31} and C_{32}hopane of Types I–V oils are between 0.81–0.58 and 0.52–0.58, respectively, indicating that the oil entered the oil-generating window (Peters et al., 2005). C_{29}22S/(22S + 22R) and ββ/(ββ + αα) regular sterane ratios did not evolve to the equilibrium endpoint, indicating that most of the oils have not exceeded the oil-generating window (Peters et al., 2005). Among them, Type I oil exhibited the highest parameter value, corresponding to the vitrinite reflectance (%Ro) value in the range of 0.82–0.86, whereas Type IV oil exhibited the lowest parameter value, corresponding to the %Ro value in the range of 0.68–0.72, and the parameter values of the other three oil types were between those of Types I and IV oils. The corresponding %Ro value is 0.78–0.80 (Huang et al., 1990). Phenanthrene and its alkyl isomers have been used in previous studies to construct several maturity parameters, such as the methylphenanthrene index (MPI1) and methylphenanthrene ratio (2-/1-MP). An empirical correspondence between such maturity parameters in oil and the reflectance of source rock vitrinite has also been established (Radke and Welte, 1983; Cassani et al., 1988; Radke, 1988). The evaluation of oil and source rock maturity based on phenicylates-related parameters has been extensively performed, and most of them have achieved good application results (Budzinski et al., 1995; Luo et al., 2016; Cheng et al., 2020). The correlation between the methylphenanthrene index and vitrinite reflectance shows a "two-stage pattern," that is, with increasing maturity, the MPI1 value of the sample increases first and then decreases (Figure 6A). The formula used to calculate vitrinite reflectance can be effectively judged using 2-/1-methylphenanthrene and 1-methylphenanthrene/phenanthrene ratios (Radke, 1988). Therefore, the equivalent R_o based on the methylphenanthrene ratio and methylphenanthrene index indicates that Types II–V oils are mature oils within the oil-generating window, which is consistent with the maturities from C_{29} regular sterane isomers. However, most of Type I oil has entered the condensate–wet gas-generating stage, which is significantly higher than the maturities indicated by the maturity parameters of steranes, indicating that there may be a mixing of early normal mature oil and later highly mature oil or natural gas in Type I oil.

Adamantanes are a series of compounds with high thermal stability in oil. Previous studies have demonstrated that an increasing degree of oil cracking would enrich adamantanes. Based on this conception, the correlation chart of the absolute content of αααC_{29} regular sterane and 3- + 4-methyldiamantanes (Dahl et al., 1999) was used to judge the degree of thermal evolution and oil cracking (Figure 6B). Normal mature oil (oil without intense cracking) has high αααC_{29} regular steranes20R content and low 3- + 4-methyldiamontadane content. With increasing maturity, αααC_{29} regular steranes20R content decreases gradually, whereas methyldiamontadane content increases gradually. When the former content drops to the detection limit, this indicates that the oil is at the start of strong cracking, that is, high-molecular-weight compounds in the oil, such as steroidal and terpenes biomarkers, are entirely cracked. At that time, the relevant content of adamantanes continues to increase with an increasing cracking degree because of their extremely high thermal stability. As shown in Figure 6, relatively high αααC_{29} regular sterane20R content was observed in Types II–V oils. Although their maturities vary slightly, no severe cracking process occurred. Most of Type I oil exhibited high maturities. The αααC_{29} regular sterane20R content of oils from Wells Hu002, Hu 2004, MN1, and MN001 was close to zero, and the content of 3- + 4-methyldiamondoadamane was high, exhibiting strong cracking characteristics. Progesteranes and progesteranes dominated the distribution characteristics of steranes with low carbon numbers. In addition, the oil samples from Wells MN001–D, TG1, and TG2 exhibit the characteristics of "mixed oil" (Dahl et al., 1999) with high content of both αααC_{29} regular sterane20R and 3- + 4-methyldiamondoadamane, reflecting the complexity of oil origin in the Huomatu anticline belt.

5.3 Biodegradation

The biodegradation of oil refers to the alteration of oil by microorganisms (Peters et al., 2005; Gong et al., 2017a). It is mainly a hydrocarbon oxidation process, which produces carbon dioxide and partially oxidized substances, such as organic acids. Because microorganisms typically consume oil compounds selectively, degraded oil is enriched in heteroatomic compounds that are difficult to modify (Huang et al., 2003, 2004; Peters et al., 2005; Wei Z. B. et al., 2007; Ross et al., 2010). Biodegraded oil will generally form an unresolved complex mixture (UCM) bulge in saturated hydrocarbon chromatography or total ion current pattern of saturated hydrocarbon chromatography–MS (Peters et al., 2005; Wei D. et al., 2007; Gong et al., 2017a). In the case of intense degradation, hopanes undergo bacterial modification to form 25-norhopanes, which are typically used as indicators of intense biodegradation (Huang et al., 2003, 2004; Peters et al., 2005; Wei Z. B. et al., 2007; Ross et al., 2010). Different oil components have different resistance to biodegradation. *N*-alkanes, as the most vulnerable series of compounds to bacterial modification, typically suffer a severe loss due to biodegradation, and their abundance is also an important index for discriminating biodegradation (Peters et al., 2005). 25-norhopanes (Figure 7) and a UCM bulge were not detected in the oil in this study, and *n*-alkanes were also abundant (Figure 5), so the oils were not modified for biodegradation.

5.4 Evaporative fractionation

After the accumulation of oil, the tectonic movement or the injection of a large amount of natural gas will redistribute the oil and gas phase in a reservoir (Gong et al., 2014, 2016; 2017b). Compounds of low-molecular-weight fractions will be dissolved in natural gas and separated from the original liquid hydrocarbon phase (Gong et al., 2014, 2016; 2017b). In a petroleum reservoir with favorable preservation conditions, subsequently charged natural gas will dilute the original hydrocarbon, making the density of petroleum lighter. In contrast, when the preservation conditions of a petroleum reservoir are poor, low-molecular-weight compounds of the original oil will dissolve in subsequently charged natural gas and migrate to a shallower reservoir to form a new gas pool or be lost (Gong et al., 2014, 2016; 2017b). Numerous geological examples of evaporative fractionation have been reported in previous studies (Matyasik et al., 2000; Zhang et al., 2011; Gong et al., 2017b). Evaporative fractionation is most likely to affect light hydrocarbon fractions in oil. Using simulation experiments and geological case studies, previous studies constructed a map plate for identifying evaporative fractionation based on the *n*-heptane/methylcyclohexane and toluene/*n*-heptane ratios (Thompson, 1987) (Figure 8A). Oil unmodified by evaporative fractionation typically has a normal range of the two ratios, whereas modified oil has relatively high toluene/*n*-heptane and low *n*-heptane/methylcyclohexane ratios due to the enrichment of aromatic and naphthene light hydrocarbon compounds (Thompson, 1987; Gong et al., 2014, 2016, 2017b). Strong evaporative fractionation can also change the distribution of *n*-alkanes (Kissin, 1987; Meulbroek et al., 1998; Losh et al., 2002). Thus, the evaporative fractionation-based modification was identified using the correlation between the carbon number distribution of n-alkanes and their molar mass (Figure 8B).

The carbon number of n-alkanes and the molar mass of oil without evaporative fractionation has a good linear relationship, whereas an inversion will be observed in evaporative fractionation-modified oil. Generally, a carbon number of inversion greater than 10 indicates strong evaporative fractionation (Losh et al., 2002; Gong et al., 2014). In this study, potential evaporative fractionation in Types I–V oils was discussed.

Type I oil, located in the Huomatu anticline belt, was subjected to evaporative fractionation of different degrees (Figures 8A,B). Oils from Wells TG1 and TG2 had the strongest modification effect, and the gas chromatographic analysis showed that the light hydrocarbon compounds in these oils had been lost. Furthermore, low-molecular-weight *n*-alkanes also suffered a strong loss. Thus, it could be concluded that the preservation conditions in the Huomatu anticline belt are poor, and a large amount of natural gas filled in the late period migrated with low-molecular-weight compounds of the original oil. In other words, the current oil reservoirs are residual. The current oil densities of the oils from Wells TG1 and TG2 are 0.86 and 0.84 g/cm^3, respectively, which is consistent with the poor reservoir preservation conditions. In contrast, oils from Wells Hu 2004, HT1, MN1, and MN001, were only weakly modified by evaporative fractionation. Only the light hydrocarbon fraction was modified, increasing the toluene/*n*-heptane ratio (Figure 8A). The low-molecular-weight *n*-alkanes of these oils are well preserved, indicating that the oil reservoirs have superior preservation conditions. When subsequently charged natural gas mixed with the original oil, the condensate oil and gas did not lose and thus heavily diluted the oil, making the oil lighter, which is supported by the current reservoir's relatively low oil densities (0.76–0.81 g/cm^3).

The light hydrocarbon fractions and *n*-alkanes of oils from GT1 and Ka6–D (Type II oil) were not subjected to intense evaporative fractionation and remained intact. Type III oil was intensively altered by evaporation fractionation. This process is most evident in oils from Wells Qi34 and QG3. The light hydrocarbon fractions and two reservoirs of low-carbon-number alkanes were severely lost, reflecting a poor preservation condition. Such a fractionation process could also be inferred from the heavy oils in these reservoirs, which are difficult to flow. Type IV oil also exhibited evaporative fractionation characteristics (Figures 8C,D). Among them, oils from Well Du50 exhibited the most intense alteration, whose light hydrocarbon fraction and low-carbon-number *n*-alkanes suffered strong losses, reflecting a poor preservation condition. The light hydrocarbon fraction in oils from Well KL1 (Type V oil) is depleted.

5.5 Comprehensive identification of oil origin and its implications for petroleum accumulation

Several oil-bearing anticlines, including Horgos, Manas, Tugulu, and Hutubi anticlines, have been formed in the Huomatu anticline belt. Light oil, condensate, and natural gas are the main types discovered in this area. The origin of oil and gas in this structural belt is the most debated (Chen et al., 2004; Kong, 2007; Liao et al., 2011; Wang et al., 2013; Chen et al., 2016c). Nevertheless, this study showed that oils in this area belong to the same genetic type because of their similar $\delta^{13}C_{bulk}$ ratios and biomarker fingerprints, which is consistent with previous studies (Chen et al., 2015b). There is a significant difference in maturity indicated by the maturity parameters of sterohopanes and phenanthrene/adamantanes in this area. In this area, there is a significant difference in the maturity parameters of sterohopanes and phenanthrene/adamantanes, indicating the charging and mixing of hydrocarbons with different maturities (Dahl et al., 1999). Oils in this study widely suffered from evaporation fractionation. However, the degree of evaporation fractionation in different anticline structures differs. The differences in reservoir preservation conditions are likely the direct cause of the current differences in the physical properties of these oils. For example, Himalayan orogeny tectonic activities form several large-scale thrust faults, resulting in poor petroleum preservation conditions in the Tugulu anticline (Tian et al., 2017). The light oil charged in the late stage was heavily lost, deteriorating the physical properties of the oil (Tian et al., 2017).

Well GT1 is located in the Gao Quan tectonic belt in the western part of the STB, and a high oil flow is produced in the Lower Cretaceous Qingshuihe Formation (Du et al., 2019). The $\delta^{13}C_{bulk}$ values and biomarker fingerprints of oils from Well GT1 were similar to those from Well Ka6 in the Aika anticline belt and other Jurassic-originated oils in the Junggar Basin (Chen et al., 2016a; Jin et al., 2019). Oils from Wells GT1 (Cretaceous reservoir) and Ka6 (Jurassic reservoir) were generated within the main oil-generating window and did not undergo intense cracking. These oils did not suffer from biodegradation during migration and accumulation. They were not subjected to obvious evaporative fractionation, indicating that the superior sealing ability of the caprocks prevented the reservoirs from a large-scale loss of oil and gas.

The accumulation process of Jurassic reservoirs in the Qigu bruchfalten is very complex and controversial (Hu et al., 2019; Lu et al., 2019). Previous studies have shown that Jurassic reservoir oils are mixed oils generated from the Permian and Jurassic source rocks (Wang et al., 2013; Chen et al., 2016b). The samples in this study also demonstrated a "mixing" characteristic based on the biomarker fingerprints and $\delta^{13}C_{bulk}$ values. The Jurassic reservoir oils in the Qigu Oilfield are all normal oils within the oil-generating window. They contain high-molecular-weight biomarkers and low methyl diadamantane content, indicating that they have not been buried to oil-cracking depths following a series of tectonic activities. These oils did not suffer from biodegradation during migration and accumulation. Evaporative fractionation is common, and poor cap preservation conditions lead to different degrees of oil and gas loss in reservoirs, resulting in high current density and waxy oils (Lu et al., 2019).

Several oil-bearing anticlines are found in the Aika anticline belt, including the Kayindike, Xihu, and Dushanzi anticlines, and shallow oil and gas reservoirs are primarily distributed in the

Neogene Shawan and the Paleogene Anjihaihe Formations (Wang et al., 2013). The origin of these oils remains controversial. Nevertheless, they have very similar biomarker fingerprints and $\delta^{13}C_{bulk}$ ratios, indicating that they belong to the same genetic type, consistent with previous studies (Chen et al., 2015b). These oils were primarily generated within the main oil-generating window and have not suffered oil cracking. Evaporative fractionation is very common and is associated with shallow burial depths and relatively poor preservation conditions. Oils from Well KL1 are also products within the oil-generating window and have not yet been cracked. The light oil components have been lost because of evaporative fractionation, reflecting poor reservoir preservation conditions. This is consistent with the tectonic background of the study area (Chen et al., 2007; Guo et al., 2011).

6 Conclusion

Five types of oils have been identified in the STB of the Junggar Basin. Type I oil is distributed in the Huomatu anticline belt, characterized by ^{13}C-depleted $\delta^{13}C_{bulk}$ ratios, low Pr/Ph ratios, high gammacerane abundance, and low diasterane content. Type II oil is distributed in the Jurassic reservoir in the Gaoquan tectonic belt and Aika anticline belt, characterized by ^{13}C-enriched $\delta^{13}C_{bulk}$ ratios, high Pr/Ph ratios, low gammacerane abundance, and high diasterane content. Type III oil is distributed in the Jurassic reservoir of Qigu bruchfalten and has similar geochemical characteristics to Type II oil despite its relatively ^{13}C-depleted $\delta^{13}C_{bulk}$ ratios and tricyclic terpene distribution pattern. TType IV oil is distributed in the shallow strata of the Aika anticline belt and has similar geochemical characteristics to Type I oil despite its relatively ^{13}C-enriched $\delta^{13}C_{bulk}$ ratios, low gammacerane content, and high Pr/Ph ratio. ype V oil is geochemically similar to Type I oil despite its relatively low C_{27} regular sterane and gammacerane content. These oils have not been subjected to biodegradation. Notable differences were observed in the evolution of maturity parameters from steroterpenes and phenanthrene/adamantanes. The former inferred normal mature oil, whereas the latter inferred strong oil cracking. Thus, a mixing process occurred in this area. The other four types of oils have normal maturities and have not suffered intense cracking. All oil types, except Type II oils, were altered by evaporative fractionation, with different alteration degrees. For Type I oils, different oil-bearing structures exhibit different evaporative fractionation, with the most severe fractionation occurring in the Tugulu anticline.

Data availability statement

The original contributions presented in the study are included in the article/Supplementary Material, further inquiries can be directed to the corresponding author.

Author contributions

ZQ: Conceptualization, Resources, Project administration HQ: Writing Original Draft, Formal analysis ZL: Writing Original Draft, Formal analysis, Methodology WM: Investigation, Data Curation RW: Investigation, Data Curation WW: Investigation, Data Curation.

Conflict of interest

All authors were employed by PetroChina.

Publisher's note

All claims expressed in this article are solely those of the authors and do not necessarily represent those of their affiliated organizations, or those of the publisher, the editors and the reviewers. Any product that may be evaluated in this article, or claim that may be made by its manufacturer, is not guaranteed or endorsed by the publisher.

References

Brassel, S. C., Fglinton, G., and Fu, J. (1985). Biological marker compounds as indicators of the depositional history of the Maoming oil shale. *Org. Geochem.* 10, 927–941.

Budzinski, H., Garrigues, P., Connan, J., Devillers, J., Domine, D., Radke, M., et al. (1995). Alkylated phenanthrene distributions as maturity and origin indicators in crude oils and rock extracts. *Geochimica Cosmochimica Acta* 59, 2043–2056. doi:10.1016/0016-7037(95)00125-5

Cao, J., Wang, X., Wei, D., Sun, P., Hu, W., Jia, D., et al. (2010). Complex petroleum migration and accumulation in central region of southern Junggar basin, Northwest China. *J. Earth Sci.* 21, 83–93. doi:10.1007/s12583-010-0004-5

Cassani, F., Gallango, O., Talukdar, S., Vallejos, C., and Ehrmann, U. (1988). Methylphenanthrene maturity index of marine source rock extracts and crude oils from the Maracaibo Basin. *Org. Geochem.* 13, 73–80. doi:10.1016/b978-0-08-037236-5.50013-0

Chen, J., Deng, C., and Wang, X. (2016c). Source of condensate oil in the middle of southern margin, Junggar Basin, NW China. *Petroleum Explor. Dev.* 43 (5), 830–840. doi:10.1016/s1876-3804(16)30108-2

Chen, J., Wang, X., and Deng, C. (2015b). Geochemcial features and classification of crude oil the southern margin of Junggar Basin, Northwestern China. *Acta Pet. Sin.* 36, 1316–1331. doi:10.7623/syxb201511001

Chen, J., Wang, X., and Deng, C. (2015a). Geochemcial features of source rocks in the southern margin, Junggar Basin, Northwestern China. *Acta Pet. Sin.* 36 (7), 768–780. doi:10.7623/syxb201507001

Chen, J., Wang, X., and Deng, C. (2016a). Investigation of typical reservoirs and occurrence regularity of crude oils in the southern margin of Junggar Basin, Northwestern China. *Acta Pet. Sin.* 37 (4), 415–429.

Chen, J., Wang, X., and Deng, C. (2016b). Oil-source correlation of typical crude oils in the southern margin, Junggar Basin, Northwestern China. *Acta Pet. Sin.* 37 (2), 160–171.

Chen, S., Qi, J., and Yu, F. (2007). Deformation characteristics in the southern margin of the Junggar Basin and their controlling factors. *Acta Geol. Sincia* 81 (2), 151–157.

Chen, S., Wang, X., and Yang, A, B. (2004). Geochemical study of forming gas reservoir in Hutubi field in zhunge'er basin. *Nat. Gas. Ind.* 24 (3), 16–18.

Cheng, B., Liu, H., Cao, Z., Wu, X., and Chen, Z. (2020). Origin of deep oil accumulations in carbonate reservoirs within the north Tarim Basin: Insights from molecular and isotopic compositions. *Org. Geochem.* 139, 103931. doi:10.1016/j.orggeochem.2019.103931

Dahl, J. E., Moldowan, J. M., Peters, K. E., Claypool, G. E., Rooney, M. A., Michael, G. E., et al. (1999). Diamondoid hydrocarbons as indicators of natural oil cracking. *Nature* 399, 54–57. doi:10.1038/19953

Du, J., Zhi, D., and Li, J. (2019). Major breakthrough of Well Gaotan 1 and exploration prospects of lower assemblage in southern margin of Junggar Basin, NW China. *Petroleum Explor. Dev.* 46, 205–215. doi:10.1016/s1876-3804(19)60003-0

Gong, D. Y., Cao, Z. L., Ni, Y. Y., Jiao, L. X., Yang, B., and Zhao, L. L. (2016). Origins of Jurassic oil reserves in the Turpan-Hami Basin, northwest China: Evidence of admixture from source and thermal maturity. *J. Petroleum Sci. Eng.* 146, 788–802. doi:10.1016/j.petrol.2016.07.025

Gong, D. Y., Li, J. Z., Ablimit, I., He, W. J., Lu, S., Liu, D. G., et al. (2018). Geochemical characteristics of natural gases related to Late Paleozoic coal measures in China. *Mar. Petroleum Geol.* 96, 474–500. doi:10.1016/j.marpetgeo.2018.06.017

Gong, D. Y., Ma, R. L., Chen, G., Ma, W. Y., Liao, L. X., Fang, C., et al. (2017a). Geochemical characteristics of biodegraded natural gas and its associated low molecular weight hydrocarbons. *J. Nat. Gas Sci. Eng.* 46, 338–349. doi:10.1016/j.jngse.2017.07.027

Gong, D. Y., Song, Y., Wei, Y. Z., Liu, C. W., Wu, Y. W., Zhang, L. J., et al. (2019). Geochemical characteristics of Carboniferous coaly source rocks and natural gases in the Southeastern Junggar Basin, NW China: Implications for new hydrocarbon explorations. *Int. J. Coal Geol.* 202, 171–189. doi:10.1016/j.coal.2018.12.006

Gong, D. Y., Wang, Z. Y., Liu, G., Chen, G., Fang, C. C., and Xiao, Z. Y. (2017b). Re-examination of the oil and gas origins in the kekeya gas condensate field, northwest China-A case study of hydrocarbon-source correlation using sophisticated geochemical methods. *Acta Geol. Sin. - Engl. Ed.* 91 (1), 186–203. doi:10.1111/1755-6724.13071

Gong, D. Y., Yu, C., Yang, X., Tao, X. W., Wu, W., and Liao, F. R. (2014). Geochemical characteristics of the condensates and their evaporative fractionation in kuqa depression of tarim basin, NW China. *Energy Explor. Exploitation* 32 (1), 191–210. doi:10.1260/0144-5987.32.1.191

Grice, K., Schouten, S., Peters, K. E., and Sinninghe Damsté, J. S. (1998). Molecular isotopic characterisation of hydrocarbon biomarkers in Palaeocene-Eocene evaporitic, lacustrine source rocks from the Jianghan Basin, China. *Org. Geochem.* 29, 1745–1764. doi:10.1016/s0146-6380(98)00075-8

Guo, C., Shen, Z., and Zhang, L. (2005). Biogenic origin characteristics of hydrocarbonsource rocks and classification of oils inthe south part of Junggar Basin, China. *J. Chengdu Univ. Technol.* 32 (3), 257–262.

Guo, Z., Wu, C., and Zhang, Z. (2011). Tectonic control on hydrocarbon accumulation and prospect for large oil-gas field exploration in the southern Junggar Basin. *Geol. J. China Univ.* 17 (2), 185–195. doi:10.16108/j.issn1006-7493.2011.02.005

He, H., Zhi, D., and Lei, D. (2019). Strategic breakthrough in Gaoquan anticline and exploration assessment on lower assemblage in the southern margin of Junggar Basin. *China Pet. Explor.* 24 (2), 137–146. doi:10.3969/j.issn.1672-7703.2019.02.001

Hu, H., Zhang, Y., and Zhuo, Q. (2019). Hydrocarbon charging history of the lower petroleum system in the southern Junggar Basin: Case study of the Qigu Oil Field. *Nat. Gas. Geosci.* 30 (4), 456–467. doi:10.11764/j.issn.1672-1926.2019.03.003

Huang, D., Li, J., and Zhang, D. (1990). Maturation sequence of continental crude oils in hydrocarbon basins in China and its signigicance. *Org. Geochem.* 16, 521–529.

Huang, H. P., Bowler, B. F. J., Oldenburg, T. B. P., and Larter, S. R. (2004). The effect of biodegradation on polycyclic aromatic hydrocarbons in reservoired oils from the Liaohe basin, NE China. *Org. Geochem.* 35, 1619–1634. doi:10.1016/j.orggeochem.2004.05.009

Huang, H. P., Bowler, B. F. J., Zhang, Z. W., Oldenburg, T. B. P., and Larter, S. R. (2003). Influence of biodegradation on carbazole and benzocarbazole distributions in oil columns from the Liaohe basin, NE China. *Org. Geochem.* 34, 951–969. doi:10.1016/s0146-6380(03)00033-0

Jin, J., Wang, F., Ren, J., Feng, W., Ma, W., and Li, S. (2019). Genesis of high-yield oil and gas in well Gaotan-1 and characteristics of source rocks in Sikeshu Sag, Junggar Basin. *Xinjiang Petrol. Geol.* 40 (2), 145–151. doi:10.7657/XJPG20190203

Kissin, Y. V. (1987). Catagenesis and composition of petroleum: Origin of *n*-alkanes and isoalkanes in petroleum crudes. *Geochimica Cosmochimica Acta* 51, 2445–2457. doi:10.1016/0016-7037(87)90296-1

Kong, X. (2007). Oil source of foothill fault-fold structural belt in Western part of the southern margin, Junggar Basin. *Petroleum Explor. Dev.* 34, 413–418.

Li, X., Shao, Y., and Li, T. (2003). Three oil-reservoir combinations in south marginal of Junggar Basin, Northwest China. *Petroleum Explor. Dev.* 30 (6), 32–34.

Li, Y., Wang, T., and Zhang, Y. (2004). Natural gas genesis and formationof gas pools in the south margin of Junggar Basin. *Acta Sedimentol. Sin.* 22 (3), 530–534.

Liao, J., Zhao, C., and Ma, W. (2011). Analysis on oil-gas origin and accumulation hydrocarbons in Hutubi gas field, Junggar Basin. *Xinjiang Geol.* 29 (4), 454–456.

Losh, S., Cathles, L., and Meulbroek, P. (2002). Gas washing of oil along a regional transect, offshore Louisiana. *Org. Geochem.* 33, 655–663. doi:10.1016/s0146-6380(02)00025-6

Lu, X., Zhao, M., Chen, Z., Li, X., Hu, H., and Zhuo, Q. (2019). Recognition of hydrocarbon accumulation in Qigu oilfield and implications for exploration in the southern margin of Junggar Basin. *Acta Petrolei Sinica* 40 (9), 1045–1058. doi:10.7623/syxb201909003

Luo, Q., George, S. C., Xu, Y., and Zhong, N. (2016). Organic geochemical characteristics of the Mesoproterozoic Hongshuizhuang Formation from northern China: Implications for thermal maturity and biological sources. *Org. Geochem.* 99, 23–37. doi:10.1016/j.orggeochem.2016.05.004

Matyasik, I., Steczko, A., and Philp, R. P. (2000). Biodegradation and migrational fractionation of oils from the Eastern Carpathians, Poland. *Org. Geochem.* 31, 1509–1523. doi:10.1016/s0146-6380(00)00103-0

Meulbroek, P., Cathles, L., III, and Whelan, J. (1998). Phase fractionation at south eugene island block 330. *Org. Geochem.* 29, 223–239. doi:10.1016/s0146-6380(98)00180-6

Moldowan, J. M., Seifert, W. K., and Gallegos, E. J. (1985). Relationship between petroleum composition and depositional environment of petroleum source rock. *AAPG Bull.* 69, 1255–1268.

Peters, K. E., Waters, C. C., and Moldowan, J. M. (2005). "The biomarker guide," in *II. Biomarkers and isotopes in petroleum system and Earth history* (New York: Cambridge University Press).

Radke, M. (1988). Application of aromatic compounds as maturity indicators in source rocks and crude oils. *Mar. Petroleum Geol.* 5, 224–236. doi:10.1016/0264-8172(88)90003-7

Radke, M., and Welte, D. H. (1983). "The methylphenanthrene index (MPI): A maturity parameter based on aromatic hydrocarbons," in *Advances in organic geochemistry*. Editor M. Bjoroy (Chichester: Wiley), 504–512.

Ross, A. S., Farrimond, P., Erdmann, M., and Larter, S. R. (2010). Geochemical compositional gradients in a mixed oil reservoir indicative of ongoing biodegradation. *Org. Geochem.* 41, 307–320. doi:10.1016/j.orggeochem.2009.09.005

Thompson, K. F. M. (1987). Fractionated aromatic petroleums and the generation of gas-condensates. *Org. Geochem.* 11, 573–590. doi:10.1016/0146-6380(87)90011-8

Tian, X., Zhuo, Q., and Zhang, J. (2017). Sealing capacity of the Tugulu Group and its significance for hydrocarbon accumulation in the lower play in the southern Junggar Basin, northwest China. *Oil Gas Geol.* 38 (2), 334–344. 10.11743/ogg20170213

Wang, P. (2011). *Analysis and geochemical application of light hydrocarbon fractionation in crude oil and source rock*. Beijing: Petroleum Industry Press.

Wang, Q., Liang, B., and Liu, X. (2021). Fluid phases and gas reservoirs of Qingshuihe Formation in well Hutan-1. *Xinjiang Pet. Geol.* 42 (6), 709–713. doi:10.7657/XJPG20220511

Wang, X., Zhi, D., and Wang, Y. (2013). *Source rocks and oil-gas geochemistry in Junggar Basin*. Beijing: Petroleum Industry Press.

Wei, D., Jia, D., and Zhao, Y. (2007a). Geochemical behaviors of crude oil in the southern margin of Junggar basin. *Oil Gas Geol.* 28 (4), 434–440.

Wei, Z. B., Moldowan, J. M., Peters, K. E., Wang, Y., and Xiang, W. (2007b). The abundance and distribution of diamondoids in biodegraded oils from the San Joaquin Valley: Implications for biodegradation of diamondoids in petroleum reservoirs. *Org. Geochem.* 38, 1910–1926. doi:10.1016/j.orggeochem.2007.07.009

Xiao, L., Lei, D., and Wei, L. (2012). Structural types and features in the west of south margin in the Junggar Basin. *Nat. Gas. Ind.* 32 (11), 36–39. 10.3787/j/issn.1000-0976.2012.11.08

Zhang, S., Su, J., Wang, X., Zhu, G., Yang, H., Liu, K., et al. (2011). Geochemistry of palaeozoic marine petroleum from the tarim basin, NW China: Part 3. Thermal cracking of liquid hydrocarbons and gas washing as the major mechanisms for deep gas condensate accumulations. *Org. Geochem.* 42, 1394–1410. doi:10.1016/j.orggeochem.2011.08.013

Zhang, W., Zhang, S., and Wang, S. (2003). Geochemical characteristics of oil and correlation of oil to resource rock in the southern edge of Junggar Basin. *J. Chengdu Univ. Technol.* 30 (4), 374–377.